Frequency-dependent mechanical damping in alloys

Raghavan Ranganathan, Yunfeng Shi, and Pawel Keblinski*
Department of Materials Science and Engineering, Rensselaer Polytechnic Institute, Troy, New York 12180, USA
(Received 14 June 2016; revised manuscript received 18 April 2017; published 19 June 2017)

We perform oscillatory shear simulations to determine the loss modulus for three solids with identical interaction yet distinct structures: ordered, random, and glassy alloys. Random and glassy alloys show more pronounced high-frequency loss in the THz regime than the ordered alloy. Ordered and random alloys exhibit a power-law decay in damping strength as frequency decreases over nearly five decades. Glassy alloy, with a limited frequency range of power-law decay, retains significant damping at low frequencies extending down to ∼100 MHz due to slow irreversible deformation of local clusters.

DOI: 10.1103/PhysRevB.95.214112

I. INTRODUCTION

Structure has traditionally played a very important role in determining a host of material properties that can be exploited to engineer materials with novel applications. Alloys, including ordered and random alloys, have been studied intensely for several decades [1,2], and their crystal structure-property relations have been well understood in general. Equally important has been the study of noncrystalline materials (such as glasses) for a wide range of structural and other applications [3,4]. The contrast in structure between the three classes of materials (ordered, random alloys, and glasses) confers diverse mechanical, thermal, and optical properties [5].

In this paper, we focus on mechanistic understanding of mechanical damping in alloys with vastly different structures. Mechanical damping, referred to alternately as dissipation [6] and internal friction [7], can be broadly understood as a measure of energy dissipated during a particular mode of deformation and has been a been a subject of focus recently. Our paper is motivated by the fact that frequency-dependent damping is an important characteristic of materials, yet it is poorly understood for hard inorganic materials. Mechanisms for damping and the inherent frequency response are strongly governed by the structural makeup of materials. In the low-frequency range, particularly in the case of soft materials, damping originates from structural relaxation and naturally depends on the frequency [8], as typically demonstrated by dynamical mechanical analysis [9]. At the higher frequencies, up to GHz, large quality factors (low damping) are desired for micromechanical and nanomechanical resonators [10–12]. Finally, in the THz range, which is relevant, e.g., for phononic interconnects [13], and in the high-frequency sound attenuation [13–15], damping arises from anharmonic phonon-phonon coupling [16,17] and is in the so-called Akhiezer regime [18].

While structural effects on mechanical properties under constant strain or stress has been extensively studied with atomic-level simulations in crystalline materials and inorganic glasses [4], a characterization of viscoelastic damping properties by such simulations is limited. Here, we study frequency-dependent damping mechanisms in materials representative of metallic alloys described by the same interatomic potential but with widely different structures, namely, ordered, random, and glassy alloys. We employ nonequilibrium (NE) molecular dynamics simulations to impose oscillatory shear deformation (referred to alternatively as "mechanical spectroscopy" in literature [6,7]) at frequencies spanning five decades.

II. SIMULATION MODELS AND METHODOLOGY

A. Model structures and interaction potential

We employ the Lennard-Jones (LJ) potential to describe binary, equiatomic ordered, random, and glassy alloys. The energy interaction parameter, ε, and the length scale parameter, σ, parametrize the interatomic energy, $E = 4\varepsilon\,[(\sigma/r)^{12} - (\sigma/r)^{6}]$. The parameters used for the two components systems are as follows: $\varepsilon_{11} = 0.15$ eV and $\sigma_{11} = 2.7$ Å, $\varepsilon_{22} = 0.5\,\varepsilon_{11}, \varepsilon_{12} = 1.5\,\varepsilon_{11}$, $\sigma_{22} = 0.91\,\sigma_{11}$, and $\sigma_{12} = 0.95\,\sigma_{11}$. The masses for the two species are made equal to 46 g/mol to simulate a system comparable to Ni-Nb 50-50 alloy [19,20]. These parameters are inspired from the classic Kob-Anderson model for binary LJ glass [21,22], with two notable differences: (a) Our system is equiatomic compared to a 80:20 atomic ratio in the original work, and (b) the σ values are modified slightly to yield stable ordered, random, and glass structures for the same set of parameters. The original Kob-Anderson parameterization yields an unstable (against glass formation) random alloy phase.

The ordered structure consists of the two atom types placed in a face-centered-cubic (fcc) lattice in alternate basis positions with the simulation cell face oriented with the (100) family of planes. Random structure is generated from a pure fcc crystal (that is, type 1 atoms) by randomly switching 50% of atoms to type 2. Glass is generated from the random phase by a melt-quench process involving heating from 300 K to 1500 K, equilibrating and quenching back to 300 K under zero hydrostatic pressure using a quench rate of 6.8 K/ps. Pair correlation functions for all three structures are shown in Fig. 1. To check for stability of the glass structure, we performed an 11 ns constant moles, constant volume, constant energy (*NVE* ensemble) simulation, and no change in the pair correlation function was observed at the end of the simulation. We note that the pair correlation function for the glass is similar to the original Kob-Anderson glass [22], and yet the same interaction parameters can describe stable ordered and random alloys as well.

*keblip@rpi.edu

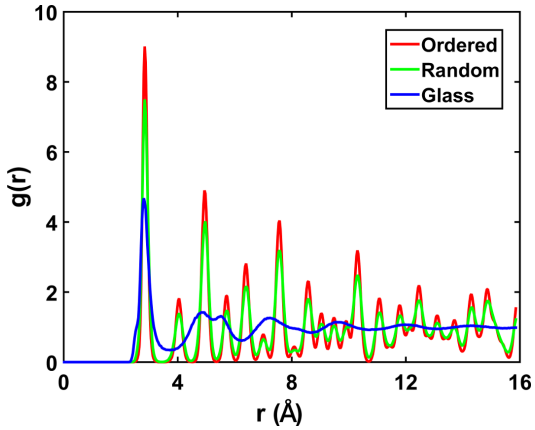

FIG. 1. Pair correlation function for ordered, random, and glassy alloys. For the glassy alloy, $g(r)$ remained unchanged over a long NVE simulation (11 ns), indicating stability.

Our standard simulation cell consists of 32000 atoms in a cubic simulation cell (box length ∼8.2 nm) with periodic boundary conditions applied along all three directions. Model structures were initially equilibrated at 300 K and at zero external pressure, before characterizing damping via NE, oscillatory shear simulations in the constant moles, constant volume, constant temperature (*NVT*) ensemble. All simulations were performed with a timestep of 0.44 fs using the Large-scale Atomic/Molecular Massively Parallel Simulator (LAMMPS) simulation package [23]. Temperature was controlled with a Nosé-Hoover thermostat [24,25] with a damping constant of 110 fs.

B. Physical characteristics of models

We have characterized the physical properties of the three model solids, including the stress-strain response under steady-state shear (to ascertain the elastic limit and shear moduli), the melting point of ordered and random alloys, and the glass transition temperature. Elastic limit for each solid was calculated from the linear portion of the shear stress-strain curve under a constant strain rate ($=10^{-3}$ ps^{-1}) shear deformation, as shown in Fig. 2, where normalized

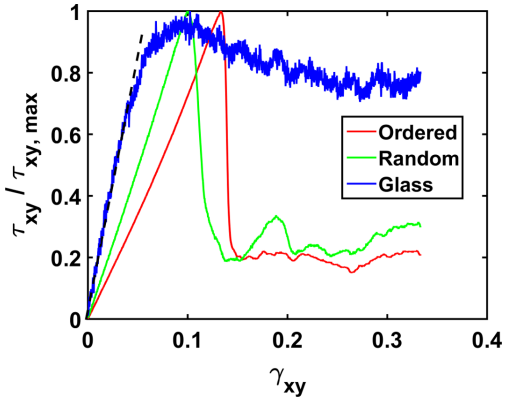

FIG. 2. Shear stress-strain plots for ordered, random, and glass alloys for determination of the elastic limit.

TABLE I. Elastic limit and shear modulus for ordered, random, and glassy alloys under a constant strain rate shear deformation.

System	Elastic limit (%)	Yield stress (GPa)	Shear modulus (GPa)
Ordered	13.2	12.0	90.9
Random	9.9	6.4	64.6
Glass	4.2	1.0	23.8

shear stress ($\tau_{xy}/\tau_{xy,\,\max}$) and shear strain ($\gamma_{xy}$) are plotted. Values of yield stress (stress at the elastic limit) and the corresponding shear moduli are tabulated in Table I. The glassy alloy exhibits ∼2 to 3 times lower elastic limit and ∼3 to 4 times lower shear modulus compared to the crystalline counterparts. We also note that ordered and random alloys exhibit yield stresses that are significantly larger (by about 12 and 6.4 times, respectively) compared to glass. The (100) planes thus constitute a strong orientation with respect to shear. Indeed, the large anisotropy for the crystals could result in quantitative differences in damping with respect to orientation as the coupling between system and the external perturbation dictates the extent of damping; however, qualitatively, the frequency dependence will still be expected to be similar. Glass also undergoes significant plastic deformation beyond a strain of ∼6%; however, the applied strain amplitude of 2% during oscillatory shear is well within the elastic limit of all three structures.

The thermodynamic melting point for ordered and random alloys were estimated by gradually heating the solid phase in a slab geometry to mimic melting from a free surface, thus avoiding superheating due to the phase change nucleation barrier [26]. The solid phase was heated from $T \sim 1$ K to $T \sim 2250$ K in steps of ~ 20 K. At the end of each heating step, constant temperature equilibration was performed for about 20 ps. Shown in Fig. 3(a) are the results for estimation of melting points. From the jump in potential energy, the melting points for ordered, and random alloys are found to be in the range 1000–1200 K.

To calculate the glass transition temperature (T_g), we heat the original random alloy to 1500 K and equilibrate the melt. Following this, the melt is quenched to a temperature of 300 K under zero external pressure, with a quench rate of 6.8 K/ps, as shown in Fig. 3(b). T_g, as estimated from the meeting point of tangents drawn from either ends of the volume-versus-temperature profile, is about 990 K.

C. Oscillatory shear methodology

A detailed description of the oscillatory shear deformation methodology is presented in our previous work [27]. Briefly, we apply a sinusoidal shear strain, $\gamma_{xy} = \gamma_o \sin(2\pi f t)$ at a shear frequency, f, by tilting a face of the simulation cell with a maximum amplitude, γ_o, of 2%. This strain is well below the elastic limit (under shear) for the ordered, random, and glass structures, which were found to be approximately 13.2%, 9.9%, and 4.2%, respectively (refer to Sec. II B. and Fig. 2).

During shear, the virial stress component (τ_{xy}) is computed and fitted to a sinusoidal profile at the same frequency as that of the applied strain but with a phase shift, δ. This allows to

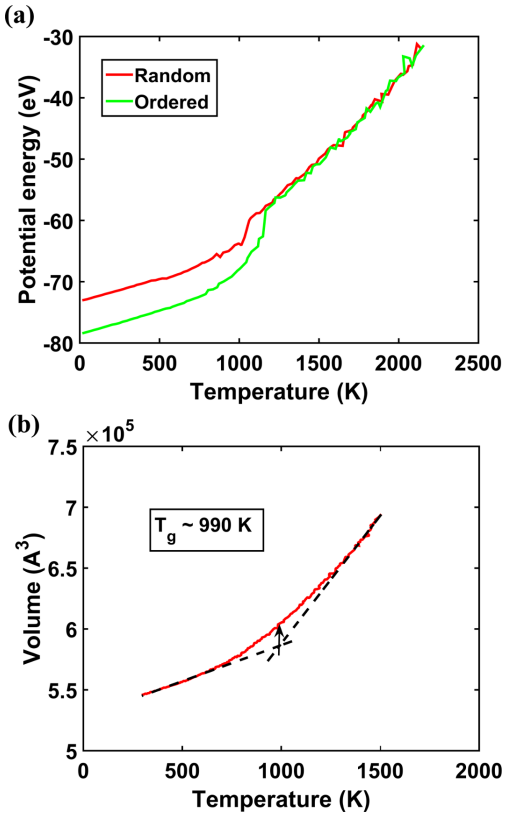

FIG. 3. (a) Variation of potential energy with temperature during slow melting of ordered and random alloys. (b) Variation of volume with temperature during quenching of melt. Glass transition temperature is estimated to be ∼990 K.

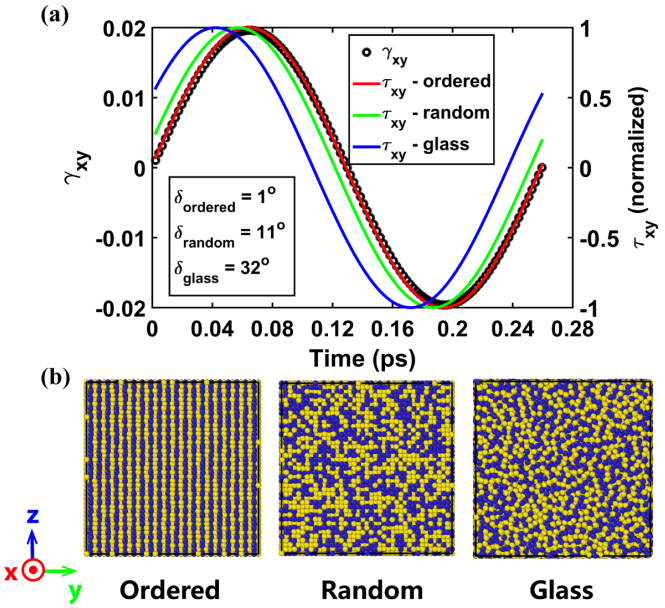

FIG. 4. (a) Averaged shear stress, τ_{xy} (solid, colored lines), and shear strain, γ_{xy} (dotted line), profiles for shear at frequency, $f \sim 3.86$ THz, for ordered, random, and glassy structures under *NVT* conditions. Stress data for the three structures have been normalized to show the effect of phase shift (indicated) clearly. (b) Atomistic snapshots of all three structures (side view).

determine the storage (G') and loss moduli (G'') constituting the complex shear modulus, $G^* = G\cos(\delta) + iG\sin(\delta)$, where $G = \tau_{xy,\,\max}/\gamma_{xy,\,\max}$. All simulations were performed at a temperature of 300 K, which is well below the glass transition temperature of 990 K (refer to Sec. II B.). At each frequency, shear deformation is averaged over multiple cycles, N, to ensure stationarity in the computed moduli. Sample high-frequency ($f \sim 1$ THz) stress-strain data obtained from oscillatory shear simulations for all three structures are shown in Fig. 4(a), where stress shown is averaged over 25 shear cycles. Atomistic snapshots for all three structures are shown in Fig. 4(b). To clearly depict the phase shift, the stress data are scaled to have the same amplitude as the strain. As seen in Fig. 4(a), the glassy alloy exhibits the largest δ of 32°, random alloy has $\delta = 11°$, while ordered structure shows negligible δ. As expected, the opposite is the case for the stress amplitude, which are 0.87 GPa, 1.3 GPa, and 1.7 GPa for glass, random, and ordered alloy structures, respectively. We are primarily interested in the dependence of loss modulus, $G'' = G\sin(\delta)$, on the structure and shear frequency, and loss modulus is used synonymously with mechanical damping in the rest of the text.

III. RESULTS AND DISCUSSION

A. Frequency-dependent loss moduli

Figure 5(a) shows the loss modulus as a function of shear frequency for the three structures. For random and glassy alloys, data were averaged for three independent structures. In the high-frequency regime ($f >\sim 0.3$ THz), the loss moduli data are averaged over $N = 400$ cycles of shear, while for lower frequencies, data are averaged over 25 cycles. We note that the computed loss moduli are largely cycle-independent (error bars in Fig. 5 are less than marker size). This is more clearly represented by Lissajous curves for variation of shear stress as a function of strain over multiple shear cycles. In the context of linear viscoelasticity, Lissajous curves are always ellipses, with the limiting cases being a straight line for perfectly elastic material ($\delta = 0°$) and a circle for perfectly viscous material ($\delta = 90°$). In Fig. 6, Lissajous curves for the three structures are plotted for a few intermediate cycles, corresponding to a shear frequency close to the peak damping frequency ($f = 2.36$ THz). Random and glassy alloys are observed to be highly stationary, i.e., show cycle-independent damping, while ordered alloy exhibits stationary damping beyond $N \sim 80$ cycles.

There are several key observations in the frequency dependence of damping, as seen in Fig. 5(a). First, there is a pronounced peak in damping in the random and glassy alloys in the high-frequency range and two somewhat less pronounced peaks in the ordered alloy. Second, upon lowering of frequency, an approximate power-law behavior in the dependence of loss modulus on shear frequency is observed [see Fig. 5(b)]. Finally, in the low-frequency range (extending down to ∼100 s of MHz), loss modulus shows a constant power-law decay for ordered and random alloys. For the glassy alloy, power-law decay persists only in a limited frequency range spanning about two decades in frequency (that overlap with the range of vibrational frequencies), below which persistent, nearly invariant damping is observed.

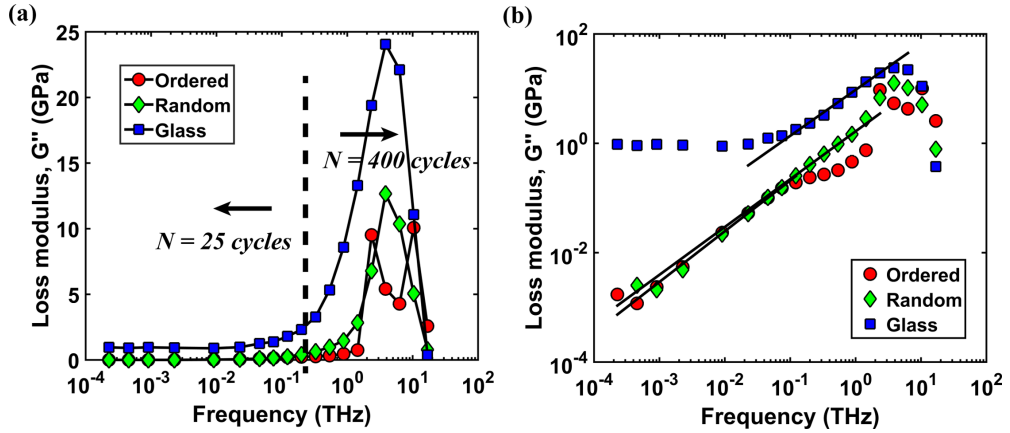

FIG. 5. (a) Frequency-sweep simulations showing the variation of loss modulus for ordered, random, and glass structures under *NVT* conditions. Data are averaged over 400 shear cycles in the high-frequency regime and over 25 cycles in intermediate and low frequencies. (b) Same data for loss moduli as in (a) but in a log-log scale, depicting power-law scaling between loss modulus and frequency (solid lines indicate power-law fits). Data are averaged over three independent structures for random and glassy alloys, and error bars are on the order of ∼0.1 GPa (smaller than marker size).

B. Damping in high and intermediate frequencies (GHz to THz)

Damping in disordered solids, such as in the random and glassy alloys in this paper, at frequencies overlapping with vibrational frequencies can be understood from the harmonic theory, as studied extensively in literature [6,28–31]. The plane wavelike shear deformation excites vibrational eigenmodes close to the driving frequency, which then act as damped harmonic oscillators [6].

To provide an explicit evidence for the damping mechanism, we performed oscillatory shear simulation where the thermostat was turned off, and thus the structure exhibited heating. We then characterized the frequency-dependent temperature, $T(f)$, according to Eq. 1 [32],

$$T(f) = T_{\mathrm{EQ}} \frac{\int_{f-\Delta f/2}^{f+\Delta f/2} C_{\mathrm{NE}}(f')df'}{\int_{f-\Delta f/2}^{f+\Delta f/2} C_{\mathrm{EQ}}(f')df'}. \quad (1)$$

Here, C_{NE} and C_{EQ} are the velocity autocorrelation functions computed during the NE shear and under equilibrium (EQ), respectively. T_{EQ} is the system temperature at EQ, equal to 350 K. Numerical integration is performed over frequency windows of length, Δf, centered at frequency, f.

Figure 7 shows the temperature of modes for two driving frequencies: (a) $f = 1.44$ THz and (b) $f = 3.85$ THz for all three structures. For all shear simulations, the starting temperature was fixed at 300 K, and velocity autocorrelation data were accumulated till the temperature reached 400 K, thereby yielding a mean temperature equal to $T_{\mathrm{EQ}} = 350$ K. As seen from the figure, for both random and glassy alloys, modes close to driving frequency have higher temperature. This phenomenon was also observed by Damart *et al.* [6] under oscillatory isostatic deformation of silica.

We note that no such clear correlation is found for the ordered system, where damping is most likely due to anharmonic coupling between vibrational modes, as observed in crystalline composites and superlattices [27]. Also interesting is the observation of two peaks in damping exhibited by the ordered alloy (Fig. 5), akin to damping in superlattices [27]; in a way, one could consider the ordered alloy to be an extreme case of superlattice with the repeating lattice period equal to one unit cell.

Additionally, glasses exhibit an excess in vibrational density of states (VDOS) near the low-frequency band, referred to commonly as the Boson peak [33], which gives rise to anamolous thermophysical properties [34]. To quantify the

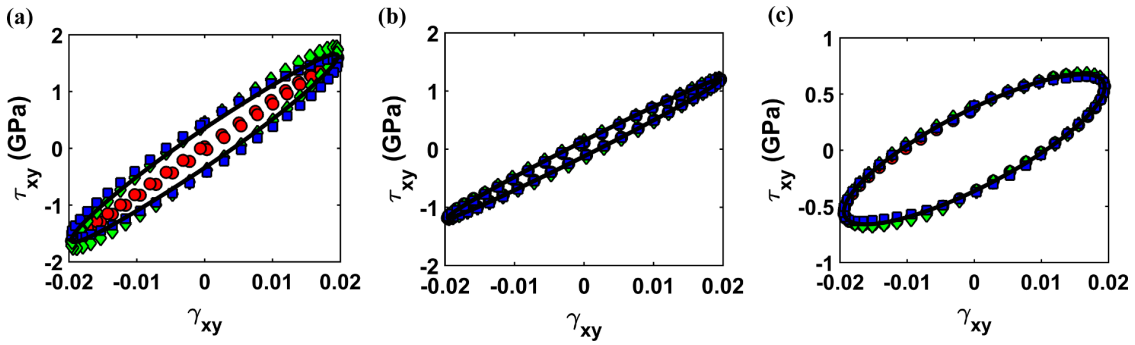

FIG. 6. Lissajous figures for (a) ordered, (b) random, and (c) glassy alloy at the maximum damping frequency of $f = 2.36$ THz. Data represented by colored markers correspond to stress-strain values from different cycle numbers, N: red (●), $N = 25$; green (♦), $N = 200$; and blue (■), $N = 400$. Solid line indicates the averaged value over $N = 400$ cycles.

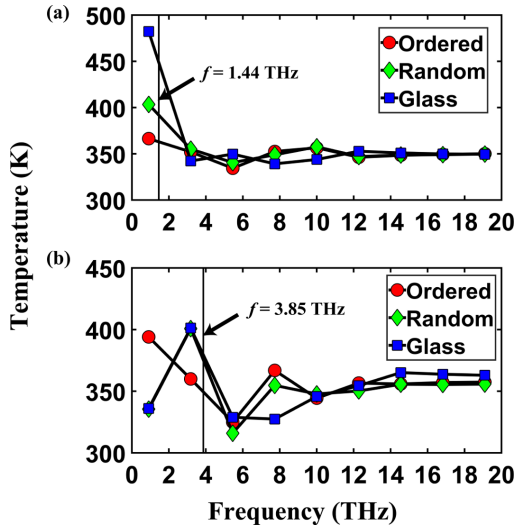

FIG. 7. Temperature of vibrational modes during shear at two frequencies, (a) $f = 1.44$ THz and (b) $f = 3.85$ THz, for ordered, random, and glassy alloys. The driving frequency is indicated by a solid line for each case. Modes closest to the driving are selectively excited for random and glassy alloys.

position of Boson peak in the model glass in relation to the peak in high-frequency damping, we computed the VDOS, $g(f)$, and the reduced DOS, $g(f)/f^2$, from the Fourier transform of the velocity autocorrelation function [35]. These are plotted in Fig. 8, along with the computed loss moduli data from Fig. 5(a). We used a system size of 256000 atoms for these calculations in order to clearly observe the Boson peak. As

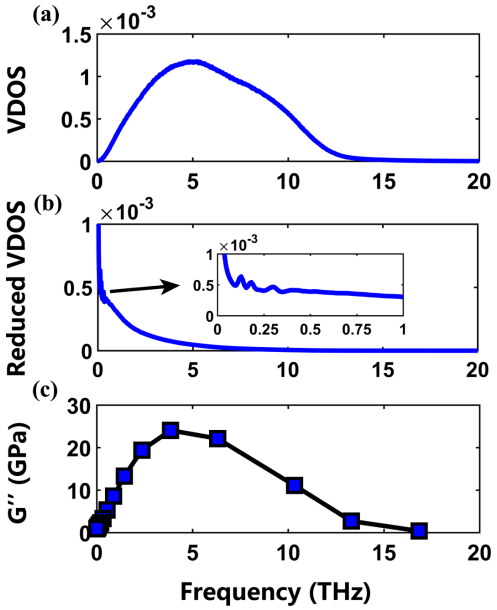

FIG. 8. Correlation between the vibrational density of states (VDOS) of the glass and the computed loss moduli. (a) VDOS, $g(f)$ of glass calculated from velocity autocorrelation function; (b) reduced VDOS computed as $g(f)/f^2$ showing a modest excess DOS (see inset) around 0.1−0.3 THz that is associated with the Boson peak. (c) Loss modulus (G'') reproduced from Fig. 5(a) for comparison.

seen from the figure, the reduced VDOS shows a modest excess around 0.1–0.3 THz, indicative of the Boson peak, below which the quasielastic peak shows a divergent behavior, as observed for many glasses [35]. Interestingly, we observe that the loss modulus begins to increase only around the Boson peak and reaches a maximum (around 4 THz) well above the Boson peak. Moreover, the frequency dependence of loss modulus [Fig. 8(c)] is seen to be approximately proportional to the DOS, across the whole frequency spectrum.

As noted earlier, upon lowering of the frequency, the loss modulus (and the phase shift) can be well-described by a power-law behavior over different frequency windows for the three structures [see Fig. 5(b)]. The power-law exponents are computed to be ∼0.93 for ordered, ∼0.87 for random, and ∼0.84 for the glassy alloy, respectively. Power-law scaling holds for about two decades of frequency for glass and for about four decades in frequency for random and ordered alloys. This is consistent with a large body of work on sound attenuation [36–39] and propagation of shock waves in viscoelastic materials [40] and damping in nanomechanical resonators [10], where a power-law scaling with respect to frequency (with an exponent ranging between 0 and 2) is observed. Indeed, widely disparate mechanisms are responsible for loss and attenuation in various viscoelastic media [36,41], and the precise mechanisms for the frequency dependence of our damping results would require separate attention.

C. Low-frequency damping in glass

Finally, we focus on the intermediate and low-frequency damping in the glassy alloy, as presented in Fig. 5 and characterized by persistent loss modulus with decreasing frequency. Such loss in glasses is associated with collective motion of atoms such as that associated with shear transformation zones and associated plastic deformation [42–44]. Such local atomic motion is usually irreversible and involves pockets of local plastic behavior (so-called *soft spots*) that manifest as shear transformation zones during onset of plastic deformation. By inspection, we verify that in the case of ordered and random alloys, the oscillatory deformation does not lead to any atomic rearrangements or defect formation at any shear frequency.

To detect and characterize such possible collective motion of atoms, we define deformation clusters as being composed of atoms that are displaced by more than 1.6 Å (equal to shear amplitude) by the end of the 25-cycle deformation, and that any atom in the cluster has at least one displaced neighbor within 3.8 Å (corresponding to the first shell of nearest neighbors).

Figure 9 shows the distribution of soft spot clusters for various frequencies in the low-frequency regime ($f \leqslant 4.5 \times 10^{-2}$ THz) for the three independent structures used in computing loss moduli, as reported in Fig. 5. Clusters are indexed by a cluster number (x axis) according to the increasing order of cluster sizes. According to Fig. 9, there is a clear trend of simultaneous increase in both cluster sizes and the number of clusters, with decreasing shear frequency. This frequency-dependent cluster size distribution could arise from two possible sources: either (a) at lower shear frequencies, the mechanism of dissipation could be dominated solely by structural rearrangements, which leads to a frequency-dependent soft spot distribution, or (b) the larger

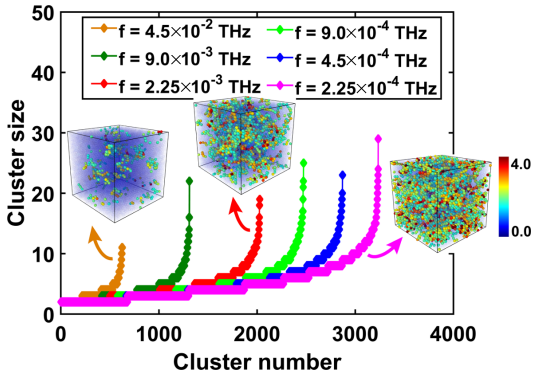

FIG. 9. Evolution of cluster size distribution at the end of 25 cycles of shear of glass for multiple shear frequencies in the low-frequency regime. Cluster size (y axis) is the number of atoms forming the soft spot, and the cluster number (x axis) is just an index of each cluster sorted by ascending order of cluster sizes. Data correspond to cluster sizes from three independent structures (same as Fig. 5). Also shown are typical snapshots of atomic regions forming the clusters for three frequencies, color-coded according to their atomic displacement (see color bar for range of displacement in Å) with respect to the initial, undeformed state. Atoms that do not contribute to the clusters are made highly transparent for clarity. Snapshots are generated using the Open Visualization Tool (OVITO) [47].

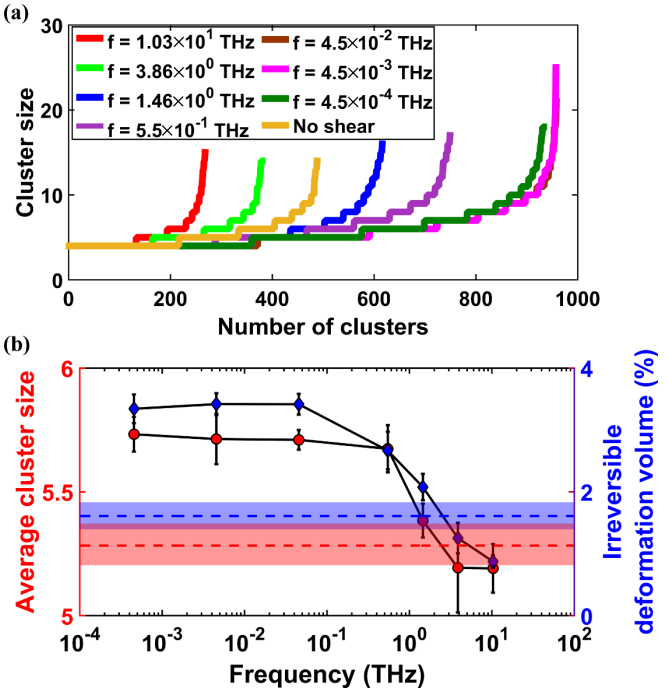

FIG. 10. Evolution of cluster sizes for oscillatory shear simulations run for a constant time (about 11 ns) instead of constant number of cycles, as shown in Fig. 9. (a) Distribution of cluster sizes for various frequencies computed for five independent glass structures. Also shown is the case corresponding to no shear, i.e., *NVT* simulation without the application of oscillatory shear, to capture the effect of aging. (b) Variation of average cluster size and percentage of atoms that contribute to irreversibly deformed clusters with frequency. The corresponding average size and deformed volume for the no shear case are indicated by dashed lines, with the range of error bars depicted by semitransparent colored bands.

amount of physical time spent during deformation for a given number of cycles could lead to larger soft spots at lower frequencies (an effect similar to aging in glasses [45,46]).

To understand the reason behind frequency-dependent distribution of soft spots more clearly, we perform oscillatory shear simulations at various frequencies in which the total simulation time is kept constant. These simulations are performed under *NVT* conditions. Coupling to a thermostat (Nosé-Hoover [24,25] in this case) was necessitated by the need to prevent significant temperature rise during shear at high frequencies over long time scales. The total time simulated is 11 ns, which corresponds to a total of five shear cycles at the lowest frequency ($f = 4.5 \times 10^{-4}$ THz) and over 100000 cycles at the highest frequency ($f = 10.3$ THz).

Shown in Fig. 10 are the cluster distribution characteristics in these *NVT* shear simulations. As seen in Fig. 10(a), which shows variation of cluster sizes, we observe a general trend of increasing cluster size and number of clusters as frequency is lowered. This particularly holds for frequencies spanning from the THz regime (where harmonic coupling is the dominant damping mechanism) to $\sim 4.5 \times 10^{-2}$ THz (which is roughly the onset of enhanced cluster formation). In some sense, the shear agitation activates different shear transformation zones, depending on the frequency of agitation. For reference, we also show cluster distribution for a no-shear case, in which we ascertain atomic displacements arising solely from aging, i.e., without the application of shear. Interestingly, the no-shear case exhibits cluster statistics intermediate to those characterizing low- and high-frequency shear. This is particularly apparent in Fig. 10(b), where the average cluster size is plotted as a function of frequency for clusters larger than four atoms. Data are averaged over five independent structures to ensure good statistics. As frequency is lowered, we observe a sharp increase in cluster sizes around 1 THz, followed by a weak variation. A similar trend is also exhibited by the total number of atoms forming the cluster (the cluster volume), also shown in Fig. 10(b). An effect concomitant with the low-frequency local deformation is the relaxation of shear stress; we observe significant stress relaxation ($\sim$56%) in glass during NVE simulations from an initially sheared state (with shear strain of 2%) over a total simulation time of 3.5 ns. Ordered and random structures, on the other hand, maintain perfect crystallinity and do not exhibit stress relaxation.

In addition to the frequency-dependent evolution of cluster sizes, we observe that the clusters exhibit significant irreversibility between cycles, i.e., atoms that form clusters remain as clusters for multiple shear cycles. As an example, in Fig. 11, we plot the total fraction of atoms that belong to clusters as a function of cycle number, N_i [Fig. 11(a)] and the fraction of cluster atoms that are identical between cycles separated by ΔN_i [Fig. 11(b)] over $N = 25$ shear cycles at $f = 4.5 \times 10^{-4}$ THz. The weakly increasing fraction of cluster atoms with N and the slow decorrelation effect of cluster atoms with cycles [the fraction of identical cluster atoms falls from $\sim$0.88 for cycles separated by $\Delta N_i = 1$ to $\sim$0.81 for $\Delta N_i = 20$, as seen in Fig. 11(b)] signify a high degree of irreversible deformation. Qualitatively similar

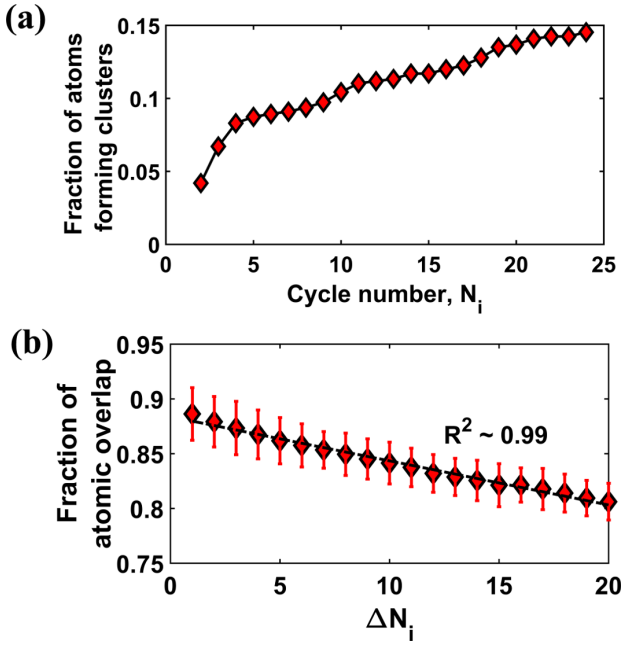

FIG. 11. Correlation between atoms forming clusters between individual cycles, N_i. Data shown here correspond to a total of $N = 25$ shear cycles at $f = 4.5 \times 10^{-4}$ THz. (a) The total fraction of atoms that contribute to clusters as a function of cycle number, N_i. (b) Fraction of atoms that are identical between cycles separated by ΔN_i.

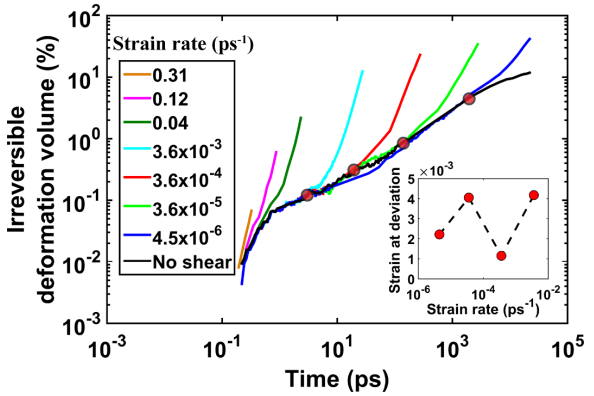

FIG. 12. Variation of deformation volume as a function of time for various strain rates during constant-rate shear deformation. The maximum shear strain for each case is 0.1. Also, shown in black is the case for no shear. The strain at which the four lowest frequencies depart from the curve for no shear (indicated by red circles) is plotted in the inset. Data are averaged over five independent structures.

behavior was observed at other shear frequencies where cluster formation is observed.

The results described above strongly indicate that low-frequency agitation of the glass structure enhances structural relaxation via local clusters that undergo irreversible deformation. The nearly invariant cluster size distribution with frequency describes the qualitative variation of loss modulus for glass in the low-frequency regime. Moreover, the clusters observed originate in a random manner, and there is less than 10% overlap between atoms contributing to clusters between any two frequencies.

In addition to oscillatory shear deformations that show frequency-dependent activation of deformation cluster sizes and cluster volume, we also observed formation of soft spots during constant strain rate shear deformation simulations performed at a range of strain rates. Figure 12 shows the fraction of deformed volume (soft spots) as a function of time for strain rates that correspond to the same set of strain rates during oscillatory shear deformation (computed as the product of strain and frequency). Data are averaged over five independent structures for good statistics. The maximum shear strain at each strain rate is set equal to 0.1. These cluster sizes and volume were observed to be time-dependent in this case, which is analogous to the frequency dependence for the case of oscillatory shear deformation. A clear trend for larger rates (lower deformation time) suppressing cluster formation akin to oscillatory shear deformation is clearly evident.

Secondly, we observe that the deformation volume for all rates collapses on to the curve for the no shear case and on to each other for low values of strain and begins to deviate at larger strains. The approximate strain at deviation from the no shear curve for the four lowest strain rates is plotted in the inset in Fig. 12 and shows that the deviation sets in approximately at a small window of strain between 0.2 and 0.4%. This further ties well with the oscillatory shear damping results in that the inverse relation between the time for formation of deformation clusters and strain rates gives rise to a nearly invariant loss modulus below a certain threshold frequency. This low-frequency damping via formation of soft spots is, in fact, also observed by us in a wide range of other model glasses as well (a topic for a separate publication), leading us to believe that it is a more universal phenomenon in glasses.

IV. CONCLUSIONS

In summary, we elucidate the mechanisms of frequency-dependent mechanical damping (as characterized by the loss moduli) in ordered and random alloys and glass, using NE, oscillatory shear, and molecular dynamics simulations. The differences in structure bring distinct dependence of damping on the applied shear frequency. At high frequencies overlapping with vibrational frequencies in the THz range, all three systems exhibit pronounced damping in the decreasing order of glass, random alloy, and ordered alloy. For glassy and random alloys, damping in this high-frequency regime is harmonic and occurs via excitation of vibrational eigenmodes close to the driving shear frequency. As we do not find a clear correlation for excitation of vibrational modes in the ordered alloy, anharmonic coupling is likely to be the dominant damping mechanism. We show that below the peak damping frequency, loss modulus can be fitted by power-law behavior over a different frequency range in each of the three structures. A unique damping mechanism in glass is observed at intermediate to low frequencies, arising from local, irreversible atomic motion, which in turn results in finite, nearly constant damping.

ACKNOWLEDGMENTS

P.K. acknowledges support from the National Science Foundation (NSF) under Grant No. CMMI-1538730. YFS acknowledges support from the NSF under Grant No. DMR-1207439. We are also grateful for the support from the Center for Computational Innovations (CCI) at Rensselaer Polytechnic Institute.

[1] N. F. Mott and H. Jones, *The Theory of the Properties of Metals and Alloys* (Dover Publications, Inc., New York, USA, 1958).
[2] F. C. Nix and W. Shockley, Rev. Mod. Phys. **10**, 1 (1938).
[3] M. F. Ashby and A. L. Greer, Scr. Mater. **54**, 321 (2006).
[4] C. A. Schuh, T. C. Hufnagel, and U. Ramamurty, Acta Mater. **55**, 4067 (2007).
[5] W. D. Callister, *Fundamentals of Materials Science and Engineering: An Interactive e·Text* (John Wiley & Sons, Somerset, NJ, 2001).
[6] T. Damart, A. Tanguy, and D. Rodney, Phys. Rev. B **95**, 054203 (2017).
[7] H. Bin Yu and K. Samwer, Phys. Rev. B **90**, 144201 (2014).
[8] H. M. Wyss, K. Miyazaki, J. Mattsson, Z. Hu, D. R. Reichman, and D. A. Weitz, Phys. Rev. Lett. **98**, 238303 (2007).
[9] W. H. Wang, Prog. Mater. Sci. **57**, 487 (2012).
[10] Q. P. Unterreithmeier, T. Faust, and J. P. Kotthaus, Phys. Rev. Lett. **105**, 027205 (2010).
[11] R. Lifshitz and M. L. Roukes, Phys. Rev. B **61**, 5600 (2000).
[12] X. Sun, K. Y. Fong, C. Xiong, W. H. P. Pernice, and H. X. Tang, Opt. Express **19**, 22316 (2011).
[13] C. Tomaras, B. Schmid, and W. Schirmacher, Phys. Rev. B **81**, 104206 (2010).
[14] J. Fabian and P. B. Allen, Phys. Rev. Lett. **82**, 1478 (1999).
[15] H. R. Schober, J. Non. Cryst. Solids **357**, 501 (2011).
[16] S. S. Iyer and R. N. Candler, Phys. Rev. Appl. **5**, 034002 (2016).
[17] K. Kunal and N. R. Aluru, Phys. Rev. B **84**, 245450 (2011).
[18] A. Akhiezer, J. Phys. USSR **1**, 277 (1939).
[19] S. Steeb and P. Lamparter, J. Non. Cryst. Solids **156-158**, 24 (1993).
[20] Y. Shi and M. L. Falk, Acta Mater. **55**, 4317 (2007).
[21] W. Kob and H. C. Andersen, Phys. Rev. Lett. **73**, 1376 (1994).
[22] W. Kob and H. C. Andersen, Phys. Rev. E **52**, 4134 (1995).
[23] S. Plimpton, J. Comput. Phys. **117**, 1 (1995).
[24] S. Nosé, J. Chem. Phys. **81**, 511 (1984).
[25] W. G. Hoover, Phys. Rev. A **31**, 1695 (1985).
[26] M. D. Kluge, J. R. Ray, and A. Rahman, Phys. Rev. B **36**, 4234 (1987).
[27] R. Ranganathan, R. Ozisik, and P. Keblinski, Compos. Part B Eng. **93**, 273 (2016).
[28] G. Ruocco, F. Sette, R. Di Leonardo, G. Monaco, M. Sampoli, T. Scopigno, and G. Viliani, Phys. Rev. Lett. **84**, 5788 (2000).
[29] S. N. Taraskin and S. R. Elliott, Phys. Rev. B **61**, 12017 (2000).
[30] P. B. Allen and J. L. Feldman, Phys. Rev. B **48**, 12581 (1993).
[31] H. Mizuno, S. Mossa, and J. Barrat, Proc. Natl. Acad. Sci. **111**, 11949 (2014).
[32] N. Shenogina, P. Keblinski, and S. Garde, J. Chem. Phys. **129**, 155105 (2008).
[33] V. K. Malinovsky and A. P. Sokolov, Solid State Commun. **57**, 757 (1986).
[34] R. C. Zeller and R. O. Pohl, Phys. Rev. B **4**, 2029 (1971).
[35] H. M. Flores-Ruiz, G. G. Naumis, and J. C. Phillips, Phys. Rev. B **82**, 214201 (2010).
[36] T. L. Szabo, J. Acoust. Soc. Am. **96**, 491 (1994).
[37] S. P. Näsholm and S. Holm, J. Acoust. Soc. Am. **130**, 3038 (2011).
[38] T. Pritz, Appl. Acoust. **65**, 1027 (2004).
[39] P. He, IEEE Trans. Ultrason. Ferroelectr. Freq. Control **45**, 114 (1998).
[40] R. Rusovici, Ph.D. dissertation, Virginia Polytechnic Institute and State University, 1999.
[41] T. L. Szabo and J. Wu, J. Acoust. Soc. Am. **107**, 2437 (2000).
[42] J. Ding, S. Patinet, M. L. Falk, Y. Cheng, and E. Ma, Proc. Natl. Acad. Sci. **111**, 14052 (2014).
[43] J. D. Ju, D. Jang, A. Nwankpa, and M. Atzmon, J. Appl. Phys. **109**, 053522 (2011).
[44] F. Shimizu, S. Ogata, and J. Li, Mater. Trans. **48**, 2923 (2007).
[45] H. Miyagawa and Y. Hiwatari, Phys. Rev. A **40**, 6007 (1989).
[46] W. Kob and J.-L. Barrat, Phys. Rev. Lett. **78**, 4581 (1997).
[47] A. Stukowski, Model. Simul. Mater. Sci. Eng. **18**, 015012 (2009).